Waning magmatic activity along the Southern Explorer Ridge revealed through fault restoration of rift topography

Anne Deschamps, M.A. Tivey, W.W. Chadwick Jr, R.W. Embley

Geochemistry Geophysics Geosystems G3

Published by AGU and the Geochemical Society

Article
Volume 14, Number 5
29 May 2013
doi:10.1002/ggge.20110
ISSN: 1525-2027

Waning magmatic activity along the Southern Explorer Ridge revealed through fault restoration of rift topography

A. Deschamps
Université de Brest, CNRS, UMR 6538 Domaines Océaniques, OSU-IUEM, Institut Universitaire Européen de La Mer, 4 Place N. Copernic, 29280, Plouzané, France (Anne.Deschamps@univ-brest.fr)

M. A. Tivey
Department of Geology and Geophysics, Woods Hole Oceanographic Institution, Woods Hole, Massachusetts, USA

W. W. Chadwick Jr.
Hatfield Marine Science Center, Oregon State University/CIMRS, Newport, Oregon, USA

R. W. Embley
NOAA, Pacific Marine Environmental Laboratory, Newport, Oregon, USA

[1] We combine high-resolution bathymetry acquired using the Autonomous Underwater Vehicle ABE with digital seafloor imagery collected using the remotely operated vehicle ROPOS across the axial valley of the Southern Explorer Ridge (SER) to infer the recent volcanic and tectonic processes. The SER is an intermediate spreading ridge located in the northeast Pacific. It hosts the Magic Mountain hydrothermal vent. We reconstruct the unfaulted seafloor terrain at SER based on calculations of the vertical displacement field and fault parameters. The vertical changes between the initial and the restored topographies reflect the integrated effects of volcanism and tectonism on relief-forming processes over the last 11,000–14,000 years. The restored topography indicates that the axial morphology evolved from a smooth constructional dome >500 m in diameter, to a fault-bounded graben, ~500 m wide and 30–70 m deep. This evolution has been accompanied by changes in eruptive rate, with deposition of voluminous lobate and sheet flows when the SER had a domed morphology, and limited-extent low-effusion rate pillow eruptions during graben development. Most of the faults shaping the present axial valley postdate the construction of the dome. Our study supports a model of cyclic volcanism at the SER with periods of effusive eruptions flooding the axial rift, centered on the broad plateau at the summit of the ridge, followed by a decrease in eruptive activity and a subsequent dominance of tectonic processes, with minor low-effusion rate eruptions confined to the axial graben. The asymmetric shape of the axial graben supports an increasing role of extensional processes, with a component of simple shear in the spreading processes.

Components: 9,800 words, 8 figures.

Keywords: Mid-ocean ridge; lava flow; spreading; axial valley; Explorer ridge; dike; cyclic.

Index Terms: 3045 Marine Geology and Geophysics: Seafloor morphology, geology, and geophysics; 3035 Marine Geology and Geophysics: Midocean ridge processes; 3080 Marine Geology and Geophysics: Submergence instruments: ROV, AUV, submersibles; 8178 Tectonophysics: Tectonics and magmatism; 8414 Volcanology: Eruption mechanisms and flow emplacement.

Received 10 December 2012; **Revised** 26 February 2013; **Accepted** 6 March 2013; **Published** 29 May 2013.

Deschamps, A., M. A. Tivey, W. W. Chadwick Jr., and R. W. Embley (2013), Waning magmatic activity along the Southern Explorer Ridge revealed through fault restoration of rift topography, *Geochem. Geophys. Geosyst.*, *14*, 1609–1625, doi:10.1002/ggge.20110.

1. Introduction

[2] Remotely operated vehicles (ROVs) and autonomous underwater vehicles (AUVs) allow more detailed investigations of mid-ocean ridges processes, as compared to previous methods such as coarser multibeam bathymetric data acquired from ships. These new high-resolution methods make it possible to produce comprehensive bathymetric maps of the seafloor at 1 m scale that highlight subtle tectonic and volcanic features including small-throw faults, tectonic fissures, eruptive fissures, flow fronts, and pillow mounds. Furthermore, digital seafloor imagery allows for these features to be identified and assessed in terms of their dimensions and other physical relationships. Given this information, we can explore questions about the origin and evolution of seafloor features using the method of restoring topography to its prefaulted morphology, as is commonly done in terrestrial environments. Below we report on a new high-resolution data set that allows us to address questions concerning the evolution of an intermediate-rate mid-ocean ridge spreading center that demonstrates how volcanic and tectonic processes have varied over time.

[3] Explorer Ridge is a ~110 km long spreading center located in the northeast Pacific Ocean off the west coast of Canada, and north of the Juan de Fuca Ridge (JdFR, Figure 1). Explorer Ridge has created the small Explorer Plate to the east and a conjugate portion of the Pacific Plate to the west over the past 3 ~ 4 Ma [*Riddihough*, 1974; *Botros and Johnson*, 1988]. The southernmost ridge segment of Explorer Ridge (Southern Explorer Ridge, SER) was known to host a large hydrothermal vent complex known as "Magic Mountain", located on the eastern shoulder of the SER spreading center near its shallowest point (~1800 m water depth), but the area had not been mapped in detail [*Tunnicliffe et al.*, 1986; *Beaudoin*, 2001]. In 2002, the summit of SER (49°46′N 130°16′W) was investigated using the R/V *Thomas G. Thompson* and underwater vehicles, as a part of the multi-investigator project under the auspices of the NOAA "Submarine Ring of Fire 2002" program [*Embley et al.*, 2002; *Yoerger et al.*, 1997, 1999; *Jakuba et al.*, 2002]. Along with ship-based mapping using the R/V *Thompson*'s 30 kHz EM300 multibeam sonar system, the primary purpose of the cruise was to carry out high-resolution mapping using the AUV ABE (Autonomous Benthic Explorer) to document the location, extent, and regional context of the Magic Mountain hydrothermal area. For this survey, ABE was equipped with the SM2000 200 kHz multibeam sonar system (< 1 m pixel size) and an Imagenex 675 kHz pencil-beam scanning sonar (< 3 m pixel size) [*Yoerger et al.*, 1997, 1999; *Deschamps et al.*, 2007] and a 3-axis fluxgate magnetometer [*Tivey et al.*, 2002]. ABE produced a very detailed bathymetry map of the "Magic Mountain" vent area, which was then used to guide a follow-up program using the Canadian ROV ROPOS [*Embley et al.*, 2002]. Details of the Magic Mountain hydrothermal field, its geological setting, and crustal magnetization are discussed in a separate manuscript. The ABE magnetic data are inconclusive on any chronological constraints because the data are strongly influenced from the hydrothermal activity within the rift valley with areas of reduced magnetization, which is punctuated by zones of strong magnetization over volcanic constructional features both within the rift and on the flanks [*Tivey et al.*, 2002].

[4] In this study, we combine the high-resolution bathymetric data with digital seafloor imagery collected during one, ~30 h long, ROPOS dive (R665) across the axial valley and the previously published seafloor photography [*Scott et al.*, 1990], to infer the recent history of volcanic and tectonic processes at the summit of the SER. We attempt to reconstruct the unfaulted seafloor terrain at SER using calculations from *Deschamps et al.* [2007], who determined the vertical displacement field and fault parameters for the SER ridge crest fault population based on a detailed analysis of the ABE high-resolution multibeam data. To perform this terrain restoration, we use the method of *De Chabalier and Avouac* [1994] who studied the deformation of the subaerial Fieale Volcano located in the Asal Rift. *Carbotte et al.* [2003] demonstrated that this method is valid for the analysis of submarine volcanic and tectonic processes at mid-ocean ridges when bathymetric data of sufficient resolution are available.

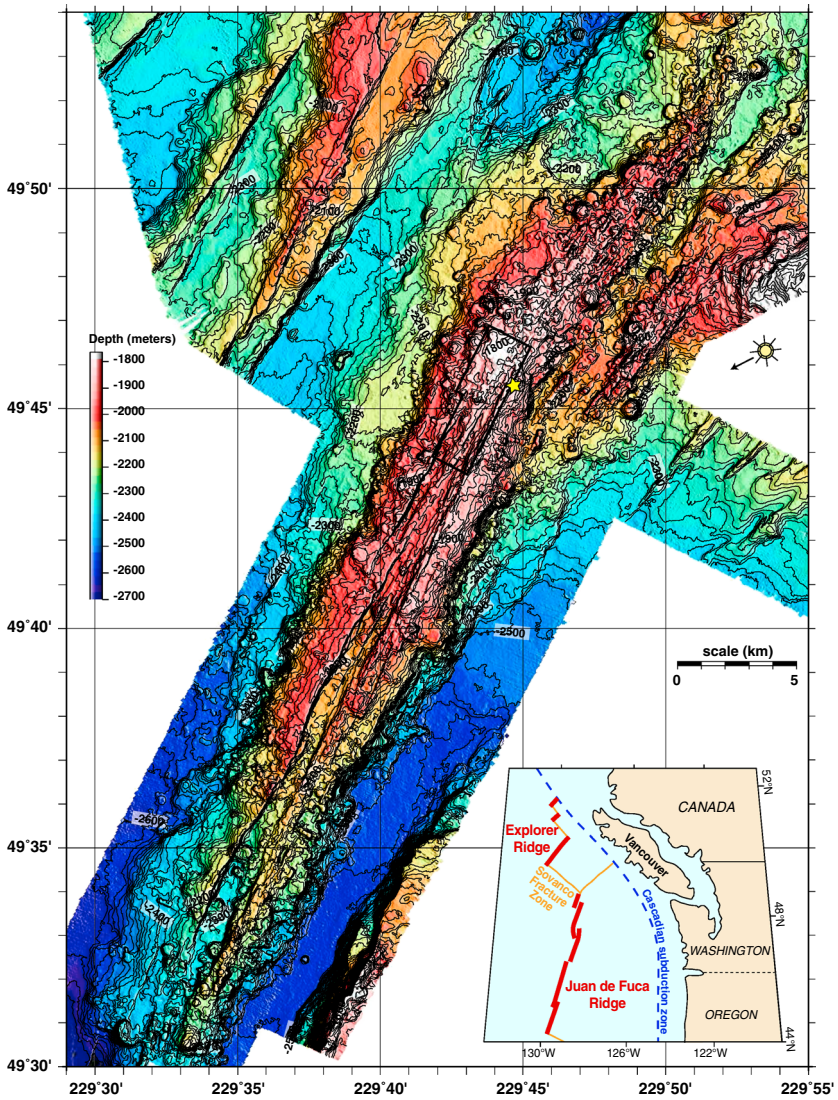

Figure 1. EM300 bathymetry of the Southern Explorer Segment. The black box indicates the study area where high-resolution bathymetry was collected and visual observations were made. Contour interval is 20 m. The star shows the position of the active Magic Mountain hydrothermal field.

We then draw conclusions about the recent evolution of the volcanic and tectonic processes that have occurred at the SER axis.

2. Geological and Petrological Setting

[5] Explorer Ridge is composed of four separate ridge segments [*Botros and Johnson*, 1988; *Beaudoin*, 2001], from south to north, the 65 km long Southern Explorer Ridge spreading segment, a 53 km long deep rift called Explorer Deep that appears to curve in an easterly overlapping spreading center arrangement with SER, and finally, two small en echelon rifts that step to the west (Explorer Rift) and terminate at the Revere-Dellwood-Wilson transform [*Davis and Riddihough*, 1982; *Braunmiller and Nábelek*, 2002]. The Explorer Ridge is bounded to the south by the Sovanco Fracture Zone, which acts as a complex right-lateral transform zone with the northern end of the Juan de Fuca Ridge and forms the southern boundary of the Explorer plate.

[6] Our study focuses on the southernmost segment of Explorer Ridge named Southern Explorer Ridge (SER) [*Michael et al.* 1989; *Beaudoin*, 2001]. The SER is a single, 5–8 km wide and 65 km long spreading segment, which is bordered by flat-floored valleys up to 7 km wide on the west and 3 km wide on the east. These valleys are bounded by fault scarps up to 800 m high, corresponding to the first occurrence of off-axis abyssal hills (Figure 1). The SER

has an inflated cross-section. The other active segments of the Explorer Ridge, located further to the northwest, are characterized by rift valleys. Seafloor spreading started at the present location of the SER ~0.3 Ma ago following an eastward ridge jump, according to *Michael et al.* [1989]. A wide axial valley is present for the southern two-thirds of its length, but the morphology of the valley evolves to a series of small grabens and fissures at the latitude of the study area, before culminating in a broad dome with no summit graben at a depth of 1740 m (at ~49°47′N) [Michael *et al.*, 1989] (Figure 1). This morphology suggests that the magma supply is greatest at the summit of the ridge and diminishes both north and south toward the segment ends [*Macdonald et al.*, 1984; *Macdonald and Fox*, 1988]. Between 49°41′N and 49°45′N, the axial valley is composed of two parallel grabens, named East and West valleys, separated by an axial volcanic ridge [*Michael et al.*, 1989]. The SER has been spreading at an intermediate-rate of 4.5 to 6 cm/yr (full rate) for 0.3 My [e.g., *Botros and Johnson*, 1988; *Braunmiller and Nábelek*, 2002].

[7] Rock samples collected in 2002 using ROV ROPOS are mainly pillow lavas, commonly with a thin manganese oxide coating. These basaltic lavas and glasses are nearly aphyric to plagioclase porphyritic, the plagioclase constituting up to 30% of the rock volume. They all are enriched mid-ocean ridge basalts (E-MORB), with K_2O ranging from 0.3 to 0.7 wt % [*Burkholder et al.*, 2003]. Normalized incompatible element patterns are light rare earth element enriched. They have a distinct peak in Nb-Ta, identical to E-MORB lavas in the West Valley Segment of the northern Juan de Fuca Ridge. Based on these analyses, *Burkholder et al.* [2003] concluded that young oceanic crust at Explorer Ridge is mainly composed of enriched mid-ocean ridge basalts, suggesting that an enriched mantle source has been present beneath the SER for a lengthy period of time. Previously, *Michael et al.* [1989] analyzed 19 samples collected along the SER axis between 49.4°N and 49.9°N. They found transitional and enriched mid-ocean ridge basalts. At the ridge summit, between 49.7°N and 49.8°N, they found incompatible element and isotopic enrichment of all basalt (E-MORB) samples that is similar to the enrichment observed in basalts typical of those associated with mantle "hotspot" plumes and anomalously voluminous basaltic volcanism [*Michael et al.*, 1989]. These results are consistent with *Scott et al.* [1990], who found that basalts from SER near the Magic Mountain site are enriched in incompatible elements K, Ti, Rb, Ba, Nb, and Zr, compared with normal depleted mid-ocean ridge basalts, and concluded that elemental ratios at SER (e.g., Nb/Zr) are characteristic of plume-type mid-ocean ridge basalts. Near the Magic Mountain site, visual observations during submersible dives show that lobate and pillow lavas predominate in the axial graben, and that sheet flows are predominant in the shallowest and flat areas surrounding the axial graben [*Scott et al.*, 1990].

[8] Extensive hydrothermal deposits and extinct sulfide chimneys along the rift valley were discovered on previous SER mapping expeditions [*Davis et al.*, 1984; *Scott et al.*, 1990]. Hydrothermal activity in the rift valley appears to have been locally extensive in the past. In the study area, two vent fields are currently active: the "Magic Mountain" area [*Tunnicliffe et al.*, 1986] and the AGOR 171 vent field, which was located through the associated water column hydrothermal plume mapped using a conductivity-temperature-depth profile [*McConachy and Scott*, 1987] (Figure 2). The Magic Mountain area remained relatively unexplored until the 2002 expedition, which provided both the local geological context of the hydrothermal sites and cleared up ambiguities on the location of the vent systems [*Embley et al.*, 2002].

3. Faulting Pattern Based on High-Resolution Bathymetry

[9] The data we present here were collected in the central part of the SER, in the vicinity of the "Magic Mountain" hydrothermal field, which is located ~8 km south of the shallowest point of the SER (Figure 1). A previous study of the deformation in this area by *Deschamps et al.* [2007] used ABE near-bottom high-resolution bathymetry acquired using a SM2000 multibeam system to characterize the fault distribution in the axial valley. In the study area, the summit of the SER is characterized by a 500 to 600 m wide and 30 to 70 m deep summit axial graben (Figure 2). The axial graben exposes numerous extensional fractures and small grabens, up to tens of meters wide, and normal faults and hybrid fractures, i.e., fractures with both an opening component perpendicular to the fracture plane and a vertical offset parallel to the fracture plane. The axial graben has a distinct asymmetric shape in relation with the nonuniform distribution of the deformation, which is accommodated by few, large faults on the eastern side of the graben compared to the western side, where there is a greater abundance of small-scale tectonic structures. As a result, the western

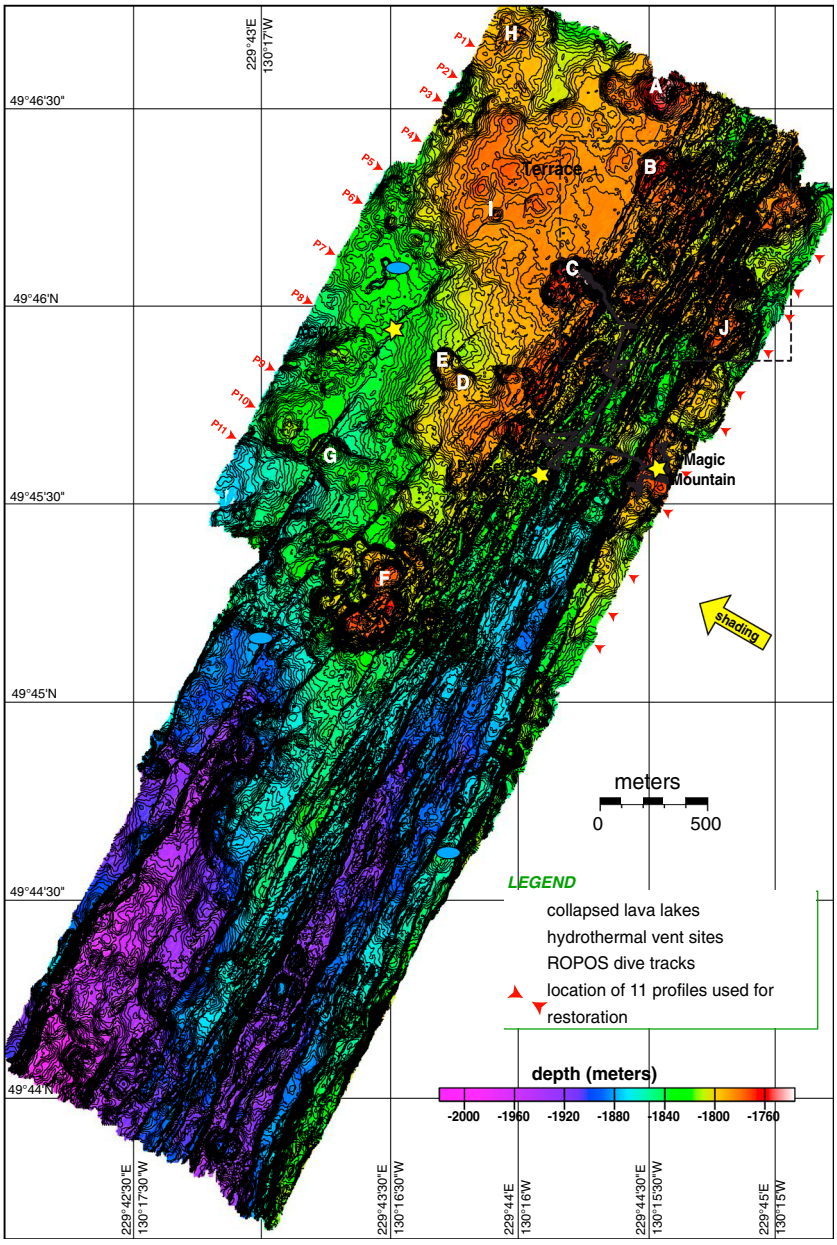

Figure 2. Bathymetry from the Imagenex sonar data (~5 m grid cell size) mounted on the ABE AUV, showing location of the 11 bathymetric profiles used for calculation of the tectonic strain in *Deschamps et al.* (2007). ROV ROPOS dive R665 track across the Southern Explorer Ridge axial valley is indicated in black. Yellow stars indicate inactive and active hydrothermal fields, and collapsed lava lake is labeled. Position of Figure 7 is indicated by dotted lines.

flank of the graben displays a more subdued morphology compared to its more sharply defined and higher standing eastern flank (Figure 2).

[10] In the northern part of the study area, fault scarps are sometimes obscured by lava flows, but in most places, their high angular aspect and their steep dip (up to 86°) suggest that they are unburied. Faults are a few meters to several kilometers long, and the average scarp height is ~10.5 m with a maximum of 63 m on the fault that bounds the eastern side of the axial summit graben. The smooth terrain west of the axial graben appears almost entirely free of faults and fissures in the high-resolution bathymetry, in striking contrast with the heavily tectonized axial graben.

4. Fault Restoration

[11] *Deschamps et al.* [2007] characterized the fault parameters and calculated the vertical displacement

field for the SER crest fault population using the high resolution ABE bathymetry data set. Here we extend the results of that study using the method of *De Chabalier and Avouac* [1994] to remove this vertical displacement field from the SER bathymetry and reconstruct the unfaulted seafloor surface. *De Chabalier and Avouac* [1994] applied their method to the deformation of Fieale Volcano of the Asal Rift (Djibouti, East Africa), a subaerial analog of a slow spreading mid-ocean ridge. To do so, they determined vertical offsets on the faults on a series of cross-sections oriented perpendicular to the rift axis, taking into account erosion at the crest and deposition at the base of scarps, the topography being linearly extrapolated onto the fault plane. They then restored the topography across the rift to a continuous surface by subtracting the vertical offsets on the faults. *Carbotte et al*. [2003] also applied this method to the southern East Pacific Rise mid-ocean ridge and showed that the method is valid for the analysis of volcanic and tectonic processes at submarine spreading centers when the resolution of bathymetric data is high enough.

[12] Using the gridded ABE SM2000 multibeam bathymetry with a 1 m cell size, we extracted 11 profiles oriented perpendicular to the axial summit graben to analyze tectonic structures and calculate tectonic strain (Figure 2) [*Deschamps et al*., 2007]. These profiles are spaced 150 to 200 m apart. In the vicinity of the Magic Mountain site, we extracted eight more profiles that are spaced only 50 m apart to reconstruct the initial three-dimensional geometry of the ridge axis near the vent site (Figure 3). Along each profile, the location and vertical offset of faults are determined, taking into account the presence of talus debris aprons and/or volcanic flows. Talus ramps are often developed at the base of active fault scarps due to their degradation, and it is important to account for them. These talus ramps are recognized by a variation in scarp dip at the foot of the fault, but of course this can also reflect other processes such as lava flow emplacement during or after faulting [see *Deschamps et al*., 2007, Figure 7B]. To take into account erosion at the crest and deposition of debris or emplacement of lava flows at the base of the scarps, the topography was linearly extrapolated onto the fault plane. To remove vertical fault displacements from the topographic data, the western end of each profile was held fixed and the seafloor was shifted up or down at each vertical offset related to a fault. To avoid bias due to talus deposition at the base of faults and erosion of the fault crests, we considered the entire height difference between the top and the bottom of fault scarps even if the slope angle is lower. Vertical relief at a fault differs from its vertical throw if the surface slopes of adjacent blocks are nonhorizontal and if fault dips are nonvertical. In our study area, however, these potential errors are minor (~3%) [see *De Chabalier and Avouac*, 1994] due to the low regional slopes of fault blocks within the study area (<5°) and the steep fault dips (60 to 86°) [*Deschamps et al*., 2007].

[13] Figures 3d and 3e show the restored surface along two cross-sections (profiles d and h, see location on Figure 3a) across the axial valley, at ~49°46′15″N and ~49°45′15″N, i.e., north and south of the Magic Mountain site, respectively. Figure 4 shows the vertically restored surface obtained by gridding the fault-shifted topography, at a 10 m grid cell size, along the eight profiles located near the Magic Mountain site. A smaller cell size would have been less useful because it would have introduced short-wavelength noise due to remaining minor fault offsets where low relief portions of faults were not accurately resolved or discrete volcanic features may have mistakenly been flagged as fault relief. The restored topography represents the topography of the ridge summit prior to the formation of the axial graben, which is approximately 11,000–14,000 years ago, considering a full spreading rate of 4.5 to 6 cm/yr and ~650 m of horizontal extension removed during the topographic restoration [e.g., *Botros and Johnson*, 1988; *Braunmiller and Nábelek*, 2002]. The restored topography has the shape of a broad dome >500 m in diameter with a gently undulating surface with several < 10 m high undulations. These bumps appear to be similar to the initial shape (i.e., before dismembering due to deformation) of the volcanic mounds observed in the study area. Some of the gentle slopes (less than 5°) may be due to tilting of the blocks that were not back-tilted during the restoration process. The largest vertical changes (~60 m) between the original and the restored topography seem to occur in the southern part of the study area, where the amount of tectonic strain is the highest (>10% assuming dip values of 70°) [*Deschamps et al*., 2007]. To the north, the restored topography is generally close to 20 m (~40 m maximum) above the former topography of the ridge summit at ~ −11,000–14,000 years.

5. Lava Morphology and Relation With Tectonic Structures

5.1. Seafloor Morphology From High-Resolution Bathymetry

[14] West of the axial summit graben, we observe a smooth and flat terrace with several subtle bumps,

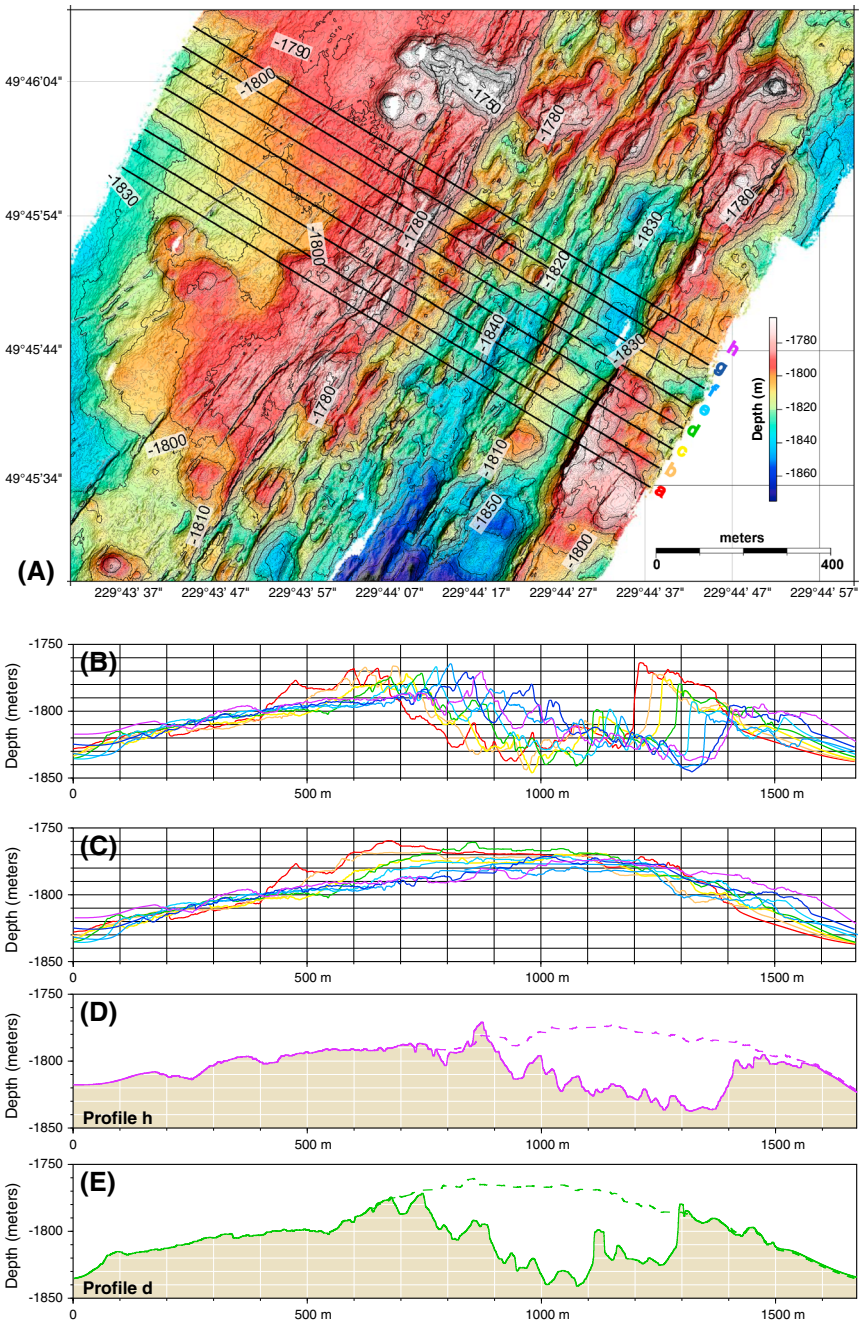

Figure 3. (A) High resolution bathymetry (~1 m grid cell size) acquired using the SM2000 multibeam sonar mounted on the ABE AUV, with the location of the eight bathymetric profiles used for topographic restoration. (B) Cross-sections of profiles a-h. (C) Topography restoration along the eight profiles in Figure 3B. (D and E) Cross-sections showing examples of original and restored profiles d and h.

each a few meters high (Figure 2). This terrace is >1.5 km in basal diameter and up to 60 m high compared to its surroundings. Such smooth topography is not related to sediment cover. Submersible dives and deep-tow photography reveal only a thin dusting of sediment covering sheet flows with a few occurrences of lobate flows [e.g., *Scott et al.*, 1990] (Figure 5). In places, sheet flows have cascaded down the west side of the axial summit graben [*Scott et al.*, 1990]. Based on ROPOS dive R665 we observed one collapsed, ~7 m deep trough (Figures 2, 5, and 6a), which corresponds to a drained lava lake that was previously identified during submersible dives [*Scott et al.*, 1990]. These submersible dives also identified lobate and sheet flows with crusts of lava only a few centimeters to

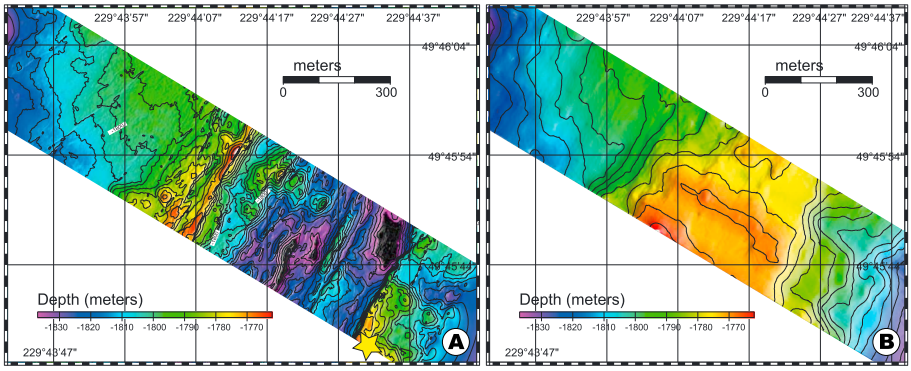

Figure 4. 2-D view of the (A) original and (B) restored bathymetry near the Magic Mountain Field. Gridding is made using the eight reconstructed profiles shown of Figure 3.

decimeters thick enclosing large voids, and on a larger scale, drained and collapsed lava lakes up to tens of meters across and tens of meters deep (see locations on Figures 3 and 5). We observe a ~4 m deep and ~100 m long lava channel going down an 8 m high dome, and several collapse pits, 6 to 30 m in diameter, within the surrounding smooth surfaced terrain (Figure 6b). The size of these collapsed troughs approaches the resolution of the data, but we do observe them in both the multibeam data set acquired using SM2000 sonar and the scanning Imagenex scanning sonar data, which confirms they are real features. We suggest that these collapse features form directly over eruptive fissures [e.g., *Fornari et al*., 1998; *White et al*., 2000; *Caress et al*., 2012].

[15] When getting closer to the axial graben, we observe an increasing number of circular to elongated mounds (mounds A to H on Figures 2 and 7), with diameters that range from a few tens of meters to 300 m. They are usually less than 25 m high, but a few reach ~45 m in height. These features have rounded summits with no craters and are accumulations of pillow and lobate lava [*Scott et al*., 1990]. They are either isolated (mound A or B on Figures 2 and 7, for example) or clustered (mounds C, F). We cannot establish the relative age of sheet flows and pillow mounds located west of the axial summit graben, but pillow mounds seem to have been built on top of the smooth terrain. We observe that most of these mounds are centered/located over the along-strike extension of fissures or grabens (mounds B, D, E, F, G). These grabens are most often narrow (<15 m in width), except for mounds B and C, which are located above a ~40 m wide graben, up to 16 m deep, with a horst in the middle. Lava partially fills the graben where mound C emerges from the northern edge of the elongated mound (Figure 7). These relations suggest that the graben formed during a dike intrusion and then was partially buried by lava when the dike reached the surface to erupt. A similar relationship was documented at the Juan de Fuca CoAxial segment in *Chadwick et al*. [2001].

[16] The pillow and lobate mounds that are observed within, or in the vicinity of the axial graben, are highly fissured and faulted (Figure 7), with highly angular morphology and steep tectonic scarps. The angular shape and steep dip (up to 86°) of fissures and faults south of 49°46′N suggest that they formed after lava mound emplacement. North of this latitude and east of the lava mounds B and C, movement on several faults was clearly synchronous with lava emplacement, as shown by their rounded shape and the more gentle dips of fault walls (Figure 7). The axial valley is highly fissured and faulted, which suggests no significant volcanic burial has occurred recently, contrary to what is commonly observed along other slow to fast-spreading mid-ocean ridges [e.g., *Deschamps et al*., 2005; *Luyendyk and Macdonald*, 1977; *Fundis et al*., 2010].

5.2. Lava Flow Morphology From Visual Observations

[17] Visual observations of lava flow morphology in the axial zone of the SER were obtained using a camera system on ROV ROPOS [*Embley et al*., 2002]. ROPOS dive R665 made a transect across the axial valley (see dive track in Figures 2 and 5). ROV observations reveal no significant differences between the various lava flows in terms of texture: all of the flows are similar in appearance and consist entirely of pillow lava with a mixture of smooth and striated textures. The pillow lavas are bulbous mounds, approximately equidimensional, with typical diameters of 0.5–2 m. Elongated pillows or

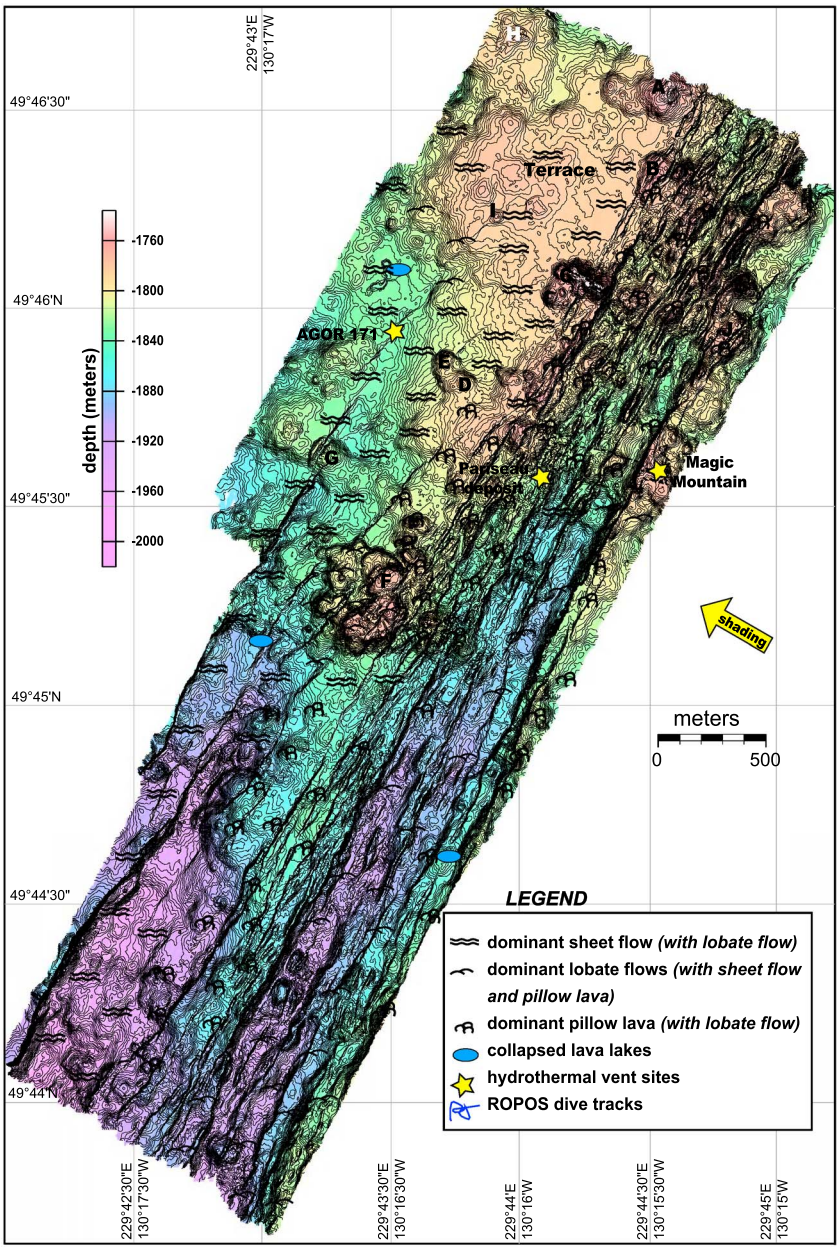

Figure 5. Bathymetry of the SER summit with the distribution of the lava morphologies from SeaMARC I side-scan sonar imagery [*Davis et al*., 1984; *Scott et al*. 1990] and visual observations during ROPOS dive R665 (track indicated in black, see Figure 8).

cylindrical flow lobes form on steeper slopes and are oriented downhill (Figure 8). We do not observe any collapsed surfaces as seen within sheet flows outside the axial valley (see above). The sedimentary cover is thin enough that the underlying rocks are exposed, except in areas of hydrothermal venting were the sediment cover reaches a few centimeters thick (Figure 8). In these areas, the lavas are typically covered by characteristic greenish-yellow and dull black hydrothermal sediments.

[18] In several places corresponding to fault traces, the terrain is marked by broken lava flow surfaces and numerous "in place" shattered pillow forms of angular basalt blocks (Figure 8). Talus rock fragments are associated with fracturing from faulting. Numerous fissures and small-throw step faults are also observed. These small-scale features are barely resolvable in the high-resolution bathymetric data (Figures 7 and 8). Rock fragments and rubble are commonly composed of angular blocks of 10 to

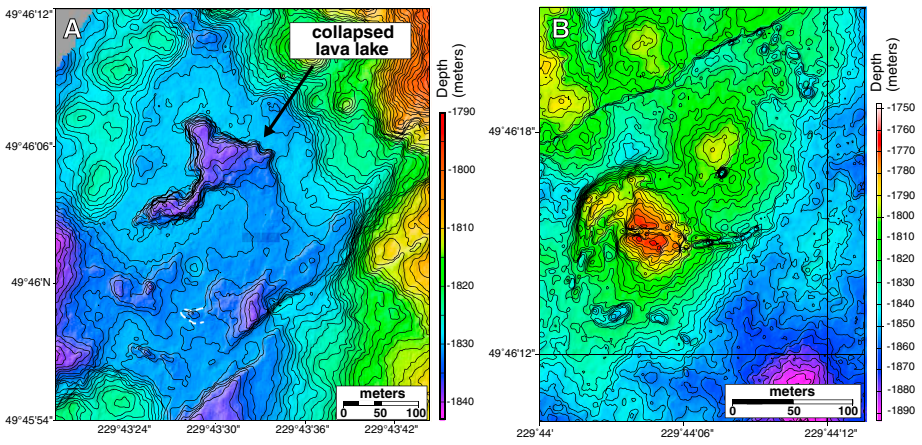

Figure 6. Detailed bathymetric maps over (A) a collapsed lava lake and (B) a lava channel. Contour interval is 1 m. Data from Imagenex scanning sonar on the ABE AUV.

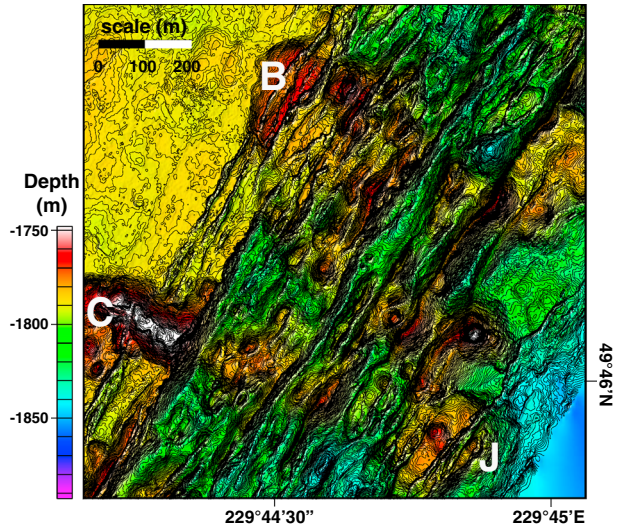

Figure 7. Bathymetry of the axial valley culmination in the vicinity of mounds B, C, and J (see Figure 2). Contour interval is 1 m. Mound C is dissected by nearly vertical, postconstructional faults [*Deschamps et al.*, 2007]. Mounds B and C are aligned with two grabens, which likely formed above the feeding dike. Interactions between faults and magmatism are clearly expressed east of mounds B and C.

60 cm in size and are mostly found at the base of these scarps. We do not observe any fault scarps that have been overrun, draped over, or covered by lava flows. It is common to see faults and fissures alternating with an intervening fault-free strip of seafloor.

6. Interpretation/Discussion

6.1. Lava Morphology and Eruption Dynamics

[19] The subcircular, 50 to 300 m in diameter, volcanic mounds in the axial valley and in its vicinity are composed of pillows and tubes. Our observations and previous ones suggest that the smooth terrain forming the crestal plateau outside the axial valley and in which collapse pits are observed are mainly composed of sheet and lobate flows. Indeed, collapse pits are indeed generally observed within lobate flows: for example, on the East Pacific Rise, 98% of collapse pits occur on lobate flows and the rest within sheet flows [*Engels et al.*, 2003]. Circular and elongated lava domes found within the axial valley and in its vicinity are composed of pillow lava. Lava mounds form when pillow lava piles up around an eruptive vent with a low-effusion rate [e.g., *Gregg and Fink*, 1995]. These pillow mounds likely represent the most recent volcanic products

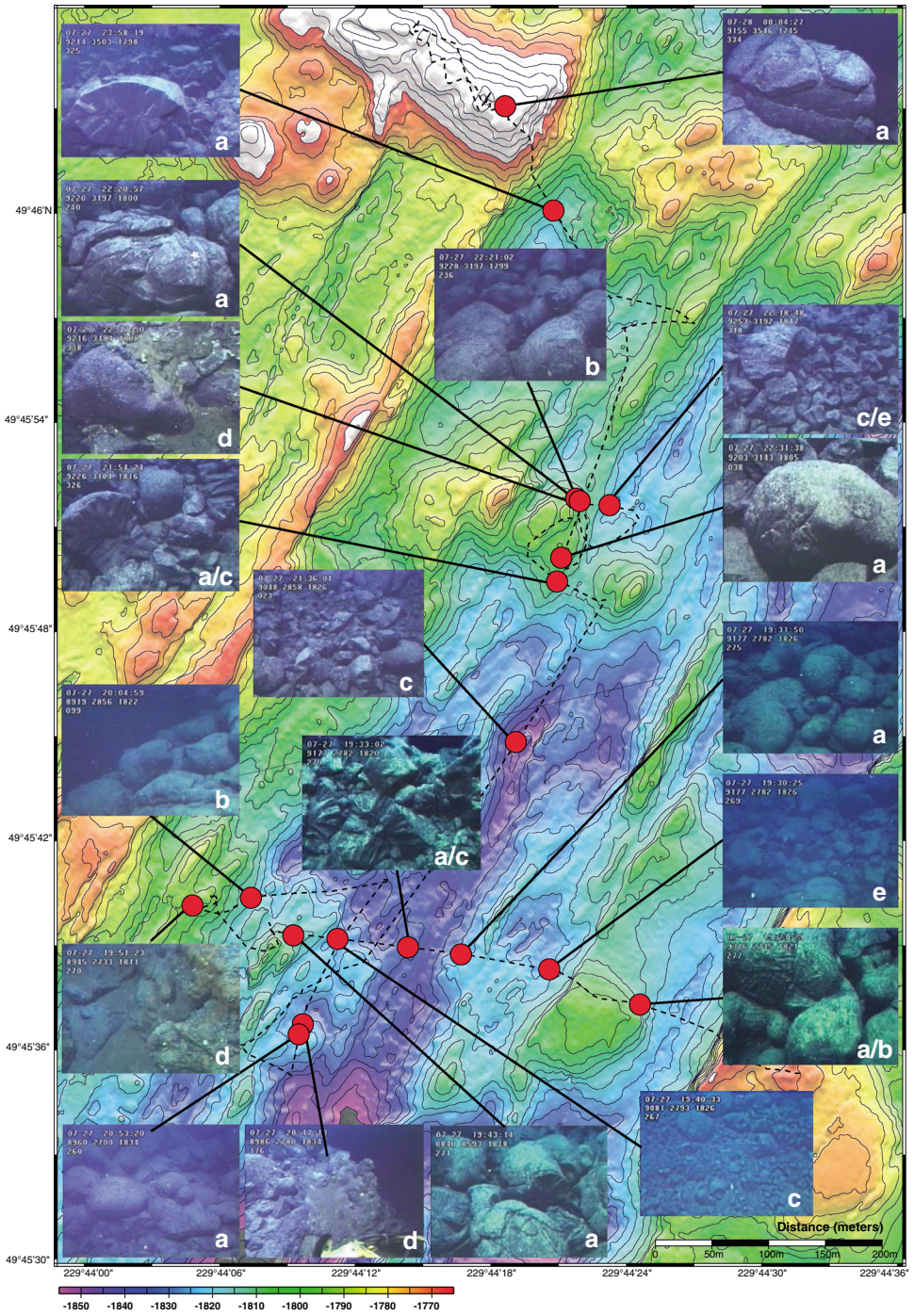

Figure 8. Bathymetric map of the SER in the vicinity of the Magic Mountain hydrothermal field, with the location of ROPOS dive R665 shown, and photographs of geologic features in the axial valley. (a) Pillow flows, (b) elongated pillows/tubes, (c) fault scarps, (d) hydrothermal deposits, and (e) breccia deposits at the base of fault and fissure scarps with well-sorted blocks.

at the SER. Consistently, it is commonly observed during dike-fed fissure eruptions on land, that soon after an eruption begins along a "curtain of fire" located above a dike, most of the fissure system shuts down, the flow of the magma localizes, and lava is discharged at a low-effusion rate from a few restricted vents for the remainder of the eruption, leading to the construction of bulbous mounds composed of pillows [e.g., *Richter et al.*, 1970; *Delaney and Pollard*, 1982; *Kappel and Ryan*, 1986; *Barone and Ryan*, 1988; *Chadwick and Embley*, 1994; *Head et al.*, 1996; *Smith et al.*, 1997].

The morphology and the localization of sheet and lobate flows and pillow mounds in the study area suggest that similar processes have occurred along the SER: an early stage of eruption produced smooth monogenetic lobate lava flows emplaced during several episodes of a long-lived eruption, 11,000 to 14,000 years ago. During the emplacement of these flows, collapse pits formed when ponded lava rapidly drained back, flowing beneath a frozen carapace that eventually collapses. At the end of the volcanic episode, pillow mounds were constructed on top of the smooth lobate flows. The fact that pillow mounds have been constructed on top of the smooth flows suggests that one or more eruption variables changed during the eruptions, probably including a waning of eruption rate [*Smith et al.*, 1997]. The fissures and narrow grabens that cleave several mounds (mounds B and C for example) probably opened above dikes. Because several of the observed pillow mounds are aligned along a single fracture system, they may relate to a single dike intrusion. Grabens indeed often form above an intruding dike, because the dike creates two zones of tension near the surface, parallel to the dike axis, but offset to either side, as observed in subaerial volcanic rift zones, [*Pollard et al.*, 1983; *Rubin and Pollard*, 1988; *Rubin*, 1992] and along mid-ocean ridges [e.g., *Chadwick and Embley*, 1998].

6.2. Topography of the Former Axial High

[20] Our model of topographic restoration near 49°45′N reveals that the SER in the vicinity of the Magic Mountain hydrothermal field formed a region of prominent domal relief, ~11,000 to 14,000 years ago. The vertical changes between the initial and the restored topography reflect the integrated effects of volcanism and tectonism on relief-forming processes [*De Chabalier and Avouac*, 1994]. The restored topography indicates that several tens of meters of inelastic deformation due to horizontal extension and faulting has taken place near the Magic Mountain hydrothermal field, and that this deformation has been more important in the eastern part of the valley, resulting in its asymmetric shape in cross-section. The restored topography has a shape of a broad dome >500 m in diameter with a gently undulating surface. The difference between the initial and the restored surface reflects, essentially, the faulting process. We do not observe any consistent evidence for inward (axis)-dipping lava flows, as might be expected for regions that have significant seafloor subsidence due to magmatic deflation, such as observed at Axial Volcano of Juan de Fuca Ridge [*Fox et al.*, 2001], at the East Pacific Rise, 18°14′S [Carbotte *et al.*, 2003], or in terrestrial volcanic systems during and after volcanic eruptions [e.g., *Sturkell and Sigmundsson*, 2000]. In addition, in this region, fault scarps generally display sharp shapes and steep dips suggesting they are unburied by volcanic flows [*Deschamps et al.*, 2007], which is confirmed by visual in situ observations. This indicates that faults postdate the lava deposition, except at latitude ~49°46′N, where there is evidence of volcanism synchronous with faulting (Figure 7).

[21] Axial topographic highs are commonly observed at fast spreading ridges and sometimes at intermediate spreading ridges. At fast spreading rates, this axial high is thought to be mainly due to the buoyancy of hot rocks and magmas beneath the ridge [e.g., *Carbotte and Macdonald*, 1994]. Consequently, as newly formed crust cools and is rafted off axis, little vestige of such an axial high remains. At intermediate-rate spreading ridges, the topographic high may also be partly due to volcanic construction. Such constructional edifices are split and preserved on the ridge flanks and form the abyssal hills [*Carbotte et al.*, 2006]. This difference in the nature of the axial high likely reflects a lithosphere strong enough to support construction of a volcanic crestal ridge at intermediate spreading rates, but only rarely at fast spreading rates [*Carbotte and Macdonald*, 1994] and/or the relative dominance of magmatism versus tectonism fast-spreading ridges, such as envisioned by *Curewitz and Karson* [1998].

6.3. Evolution of the SER as Revealed by its Morphology

[22] Our study provides new insights into the evolution of SER morphology since ~11,000–14,000 years ago. The axial morphology clearly evolved from a "dome-shaped" feature to a fault-bounded asymmetric axial graben, ~500 m wide and ~30–70 m deep. This evolution appears to have been accompanied by changes in the magma supply and eruption style through time both within the axial valley and adjacent to it. The abundance of pillow lava mounds in the valley indicates that the fissure eruptions at this location occurred at a relatively low effusion rate, but were of sufficient duration to focus and produce a line of volcanic edifices [*White et al.*, 2000]. Far from the axial graben, we observe voluminous smooth lobate and sheet flows, collapsed features, and few occurrences of pillow lava. This suggests that high effusion rate eruptions were common at the time the SER had a dome-shaped morphology. The limited number of small lava mounds (2 to 6 m in height and 40 to 60 m in diameter) formed on top

of this smooth terrain suggests that fissure eruptions rarely focused to point sources for extended periods, at lower effusion rates.

[23] The undeformed appearance of the axial summit plateau may be due either to resurfacing by eruptions onto the ridge flanks outside the axial valley, or by "escaping" the deformation during a period of near-axis faulting after the formation of the broad plateau. Along the intermediate-spreading Cleft segment, the fact that lavas that fill the axial valley are younger than the flows on the ridge flank led *Kappel and Ryan* [1986] to hypothesize that the flows on the ridge flanks formed during a previous episode of robust volcanism. Similarly, *Smith et al.* [1994] based on submersible observations and sampling at Cleft, proposed that robust magmatism typical of fast-spreading ridges alternates with periods of nearly amagmatic extension with few eruptions at a low effusion rate. This kind of waxing and waning of magmatic phases has also been proposed to occur along the EPR [e.g., *Fornari et al*., 1998; *Cormier et al*., 2003]. We suggest that a similar model best explains our observations on the SER, and that the lava flows that comprise the restored ridge dome were erupted on-axis during a period of robust magmatism, and that the lava flows that pave the axial valley floor and form small mounds were formed during a period of nearly amagmatic extension. The spatial pattern of sediment cover, the extent of the smooth terrain near the ridge axis, and the cross-cutting relationships between the smooth terrain and near-axis faults and pillow mounds suggest that at the SER, the smooth textured lavas were erupted within a short but waxing phase of activity, which was then followed by a period of less voluminous eruptions with a lower eruption rate. The axial summit graben may have initiated during this waning phase under continuous tectonic stretching, or, if already existing, deepened by downfaulting of the inflated summit accompanied by intense fissuring. This collapse probably happened after a decrease in the magma supply had occurred. Our ridge topography restoration indicates that the formation of the axial graben is mainly due to normal faulting and tectonic extension processes. As a consequence, the SER is likely currently splitting tectonically. This hypothesis is corroborated by the asymmetric shape of the graben, which reflects a component of simple shear in the extensional process, according to the model of *Wernicke* [1985]. Such a half graben-like structure is typical in the early stages of deformation within rift zones [*Gudmundsson*, 1992]. Due to ongoing predominant tectonism, this axial depression may continue to widen until a new magmatic phase will initiate the construction of a new dome.

[24] The evolution of SER topography over the past 11,000–14,000 years also seems to be accompanied with a concomitant evolution in hydrothermal activity. Many vestiges of inactive hydrothermal vents are observed within this valley, the remaining active vent site in this area being the Magic Mountain field, located on the east shoulder of the valley, suggesting that the hydrothermal activity has decreased as magmatism waned and tectonism became dominant.

[25] The results of this study support the hypothesis that there is no continuous magma supply at the SER, but rather phases of waxing and waning of magmatism, and associated hydrothermal activity, with cycles longer than 11,000–14,000 years. The existence of such volcano-tectonic cycles at other spreading centers has been inferred by numerous authors, based on observations and models [e.g., *Parson et al*., 1993; *Tucholke and Lin*, 1994; *Smith et al*., 1994; *Wilcock and Delaney*, 1996; *Perfit and Chadwick*, 1998; *Briais et al*., 2000]. As to the cycle duration, *Sauter et al.* [1991] inferred a periodicity of about 0.25 Ma for the volcano-tectonic cycles on the intermediate-spreading South-East Indian Ridge. *Briais et al.* [2000] inferred magmatic cycles to be less than 1 Ma at the slow-spreading Mid-Atlantic Ridge, 27–30°N, for example.

[26] Our results contrast with those of *Carbotte et al*. [2006] and *Stakes et al*. [2006], who interpreted seismic observations of crustal structure to suggest that the large-scale axial rift topography on the JdFR reflects subcontinuous dike-induced deformation rather than alternating phases of magmatism and tectonic extension. In their model, the evolving axial topography results from progressive rifting, deepening, and broadening of the axial valley due to dike intrusions alone. Their model for the JdFR suggests a relatively constant effusion rate through time with the axial valley floor of the JdFR displaying abundant lobate, sheet and massive flows, reflecting high effusion rates during axial valley formation. They also observe that the most recent axial eruptions are more primitive (higher MgO) whereas in the case of a decrease of magmatic activity, extraction of magma would be expected to occur from magma pockets beneath the segment center and lead to low-effusion eruptions of more chemically evolved, incompatible element-depleted basalts [e.g., *Briais et al*., 2000; *Stakes et al*., 2006]. In addition, dike-induced axial valley formation should result in a graben that is symmetrical, as observed by

Carbotte et al. [2006] along the JdFR. However, in the case of the SER, the axial graben is highly asymmetric, as shown by cross-sections in Figure 3, which likely reflects a component of simple shear in the extensional process, according to the model of *Wernicke* [1985]. Deformation on faults and shear zones is indeed inherently asymmetric [e.g., *Wernicke and Burchfiel*, 1982; *Wernicke*, 1985; *Lister et al*., 1986; *Mutter et al*., 1989; *Boillot et al*., 1992; *Brun and Beslier*, 1996], extension of the upper crust through faulting often leads to half-graben development, bounded on one side by a master fault, and on the other by a zone of more distributed deformation taken up by minor faults [e.g., *Bally*, 1982; *Morley*, 1995; *Patton et al*., 1994].

[27] *Cousens et al*. [1984] and *Scott et al*. [1990] found an incompatible element enrichment of basalts from the SER study area indicating that the ridge likely lies above a hotspot. The incompatible trace element analysis indicates that the mantle source of the SER's basalts is heterogeneous on a multikilometer scale [*Michael*, 1988]. Sr isotopic ratios are correlated with the incompatible elements ratios, but the isotopic enrichment is very subdued, which suggests that incompatible element enrichment occurred relatively recently [*Michael et al*., 1985]. Consistently, basalts collected 15 km off-axis (i.e., ~0.7 Ma old), west of the ridge axis have a depleted Normal Mid-Ocean Ridge Basalt signature, indicating that enriched material has been introduced only recently into the source region. *Michael et al*. [1989] thus concluded that the enrichment of MORB in the whole region (north of Axial seamount on the Juan de Fuca Ridge) is likely related to intermittent pulses of magma generation from the deep mantle, which enriches the upper mantle, in contrast to a more constant and persistent hotspot. In this regard, the cyclic evolution of the SER documented in this study may be related to such intermittent pulses in relation with variable hotspot activity. Nevertheless, one can expect the evolution time scale of the magmatic activity along a ridge segment not to be entirely identical or in phase with the activity time scale of a hotspot, the latter (i.e., diffuse or intermittent pulses of magma generation from the deep mantle) being on a longer time scale. Along- and across-axis lava sampling for dating and geochemical studies would be necessary to better characterize the variability of the magma composition in space and time and for a better identification of the magmatic pulses along the ridge and their relation with the hotspot activity.

7. Conclusions

[28] The geology and structure of the Southern Explorer Ridge have been examined using high-resolution multibeam sonar systems mounted on an AUV, combined with visual observations from an ROV. The high-resolution bathymetry coupled with in situ observations on near-axis and flank regions provide a detailed picture of the morphology of the most recent upper crust created at the SER summit, and were used to interpret its recent magmato-tectonic history.

[29] Topography restoration reveals that approximately 11,000 to 14,000 years ago, the ridge was characterized by widespread volcanism that formed a wide crestal plateau that is now split by the present axial valley. Our observations support a model of cyclic volcanism at the Southern Explorer Ridge, in which a discontinuous magma supply creates alternating phases of waxing and waning of magmatism. According to this model, a period of intense effusive volcanism flooded the axial rift with sheet and lobate lava flows, and formed a several kilometer-wide plateau at the ridge summit. At this time, volcanic construction dominated over tectonic strain in shaping the morphology of the segment. This episode was subsequently followed by a decrease in eruptive volume and in the distance travelled by the lava flows, the most recent eruptions being smaller and confined to the axial graben. During this waning phase, the deepening and widening of the axial graben has been accompanied by a concomitant decrease in hydrothermal activity. This tectonically dominated episode probably initiated in the southern part of the SER, where the rift is presently deeper and wider and propagated northward. The role of tectonic processes in shaping the present day graben is underlined by its asymmetric shape reflecting a component of simple shear in the extensional processes.

[30] Such discontinuous magma supply may relate to the periodic disappearance or deepening of the magma source during ongoing spreading due to plate divergence. During a waning phase, the floor of the axial valley is not necessarily devoid of volcanic activity, but the volumes and rates of eruption are significantly reduced, leading to low effusion-rate eruptions from point sources. Such intermittent magmatic and tectonic processes likely result in the alternating central-high/central-low morphology observed in the shape of abyssal hills in the vicinity of the SER, and alternating phases of intense and moribund hydrothermal activity. Whether or not this cyclicity is due to intermittent

pulses of magma generation from the deep mantle in relation with the hotspot located in the vicinity of the ridge axis is not clear.

[31] Our hypothesis contrasts with that of *Carbotte et al*. [2006], who suggested that at the Juan de Fuca Ridge axial rift topography is related to dike-induced deformation rather than tectono-magmatic cycles, based on the fact that the axial graben width and height diminish where axial magmatic reflectors disappear, and on the observation of high-rate effusive lava flooring the axial valleys. In such a model, the bounding ridges are relicts of an axial volcanic ridge that is subsequently split by dike-induced faulting and rafted onto the ridge flanks.

[32] Additional geochemical studies and dating of well-identified lava flows at the SER ridge axis and flanks would help to distinguish between these two hypotheses by establishing a relative chronology of magmatic events in this area in relation with the degree of fractionation of the basalts. Seismic profiles would also help to document the depth of an axial magma chamber at Southern Explorer Ridge.

Acknowledgments

[33] Funding for the 2002 Submarine Ring of Fire expedition was from the NOAA Ocean Exploration Program and NOAA's Pacific Marine Environmental Laboratory. We thank Ed Baker (co-chief scientist) and the science team and the personnel of the R/V *Thomas G. Thompson* for their support during the cruise. The success of this expedition is largely due to the ABE team led by D. Yoerger and A. Bradley who provided technical and excellent operational support. We thank M. Jakuba who developed the SM2000 data processing tool, which was used for the first time on this expedition. PMEL contribution number 3945. This work was supported by a Woods Hole Oceanographic Institution Post-doctoral Scholarship, CNRS and Université de Bretagne Occidentale, France.

References

Bally, A. W. (1982), Musings over sedimentary basin evolution, *Philos. Trans. R. Soc. London, Ser. A*, *305*, 325–328.

Barone, A. M., and W. B. F. Ryan (1988), Along-axis Variations within the Plate Boundary Zone ofthe Southern Segment of the Endeavour Ridge, *J. Geophys. Res.*, *93* (B7), 7856–7868.

Beaudoin, Y. C. (2001), Physiology, geology and geochemistry of the southern explorer ridge seafloor hydrothermal site using an integrated GIS database and 3D modeling. Thesis (M.Sc.), University of Toronto, https://tspace.library.utoronto.ca/bitstream/1807/16006/1/MQ58812.pdf.

Boillot, G., M.-O. Beslier, and M. Comas (1992), Seismic image of undercrusted serpentine beneath a rifted margin, *Terra Nova*, *4*, 25–33.

Botros, M., and H. P. Johnson (1988), Tectonic evolution of the Explorer-Northern Juan de Fuca region from 8 Ma to the present, *J. Geophys. Res.*, *93*, 10,421–10,437.

Braunmiller, J., and J. Nábelek (2002), Seismotectonics of the Explorer region, *J. Geophys. Res.*, *107*. doi:10.1029/2001JB000220.

Briais, A., H. Sloan, L. M. Parson, and B. J. Murton (2000), Accretionary processes in the axial valley of the Mid-Atlantic Ridge 27°-30°N from TOBI side-scan sonar images, *Mar. Geophys. Res.*, *21*, 87–119.

Brun, J. P., and M. O. Beslier (1996), Mantle exhumation at passive margins, *Earth Planet. Sci. Lett.*, *142*, 161–173.

Burkholder, M., M. Scarpelli, and B. L. Cousens (2003), Geochemistry of basalts and sulphides from the Magic Mountain Hydrothermal Field, Explorer Ridge, Northeast Pacific Ocean, *GAC-MAC-SEG Joint Annual Meeting*, *Vancouver*, *British Columbia*, *May 25–28*, Abstract with Programs, Vol. 28, Abstract number 418.

Carbotte, S. M., and K. C. Macdonald (1994), Comparison of seafloor tectonic fabric at intermediate, fast, and super fast spreading ridges: Influence of spreading rate, plate motions, and ridge segmentation on fault patterns, *J. Geophys. Res.*, *99*, 13,609–13,631.

Carbotte, S. M., R. S. Detrick, A. Harding, J. P. Canales, J. Babcock, G. Kent, E. Van Ark, M. Nedimovic, and J. Diebold (2006), Rift topography linked to magmatism at the intermediate spreading Juan de Fuca Ridge, *Geology*, *34*(299–212), 197.

Carbotte, S. M., W. B. F. Ryan, W. Jin, M. H. Cormier, E. Bergmanis, J. Sinton, and S. White (2003), Magmatic subsidence of the East Pacific Rise (EPR) at 18°14′S revealed through fault restoration of ridge crest bathymetry, *Geochem. Geophys. Geosyst.*, *4*(1008). doi:10.1029/2002GC000337.

Caress, D. W., D. A. Clague, J. B. Paduan, J. Martin, B. Dreyer, W. W. Jr. Chadwick, A. Denny, and D. S. Kelley (2012), Repeat bathymetric surveys at 1-metre resolution of lava flows erupted at Axial Seamount in April 2011, *Nature Geosci.*, *5*(7), 483–488.

Chadwick, W., and R. Embley (1994), Lava flows from a mid-1980s submarine eruption on the Cleft segment, Juan de Fuca Ridge, *J. Geophys. Res.*, *99*(B3), doi:10.1029/93JB02041.

Chadwick, W. W., Jr., and R. W. Embley (1998), Graben formation associated with recent dike intrusions and volcanic eruptions on the mid-ocean ridge, *J. Geophys. Res.*, *103*, 9807–9825.

Chadwick, W. W., Jr., D.S. Scheirer, R. W. Embley, and H. P. Johnson (2001), High-resolution bathymetric surveys using scanning sonars: lava morphology, hydrothermal vents, and geologic structure at recent eruption sites on the Juan de Fuca Ridge, *J. Geophys. Res.*, *106*, 16,075–16,099.

Chadwick, W. W., Jr., R. P. Dziak, J. H. Haxel, R. W. Embley, and H. Matsumoto (2012), Submarine landslide triggered by volcanic eruption recorded by in-situ hydrophone, *Geology*, *40*(1), 51–54. doi:10.1130/G32495.1.

Cormier, M. -H., W. B. F. Ryan, K. Shah, J. Wen, A. M. Bradley, and D. R. Yoerger (2003), Waxing and waning volcanism along the East Pacific Rise on a millennium time scale, *Geology*, *31*(7), 633–636, ISSN 0091–7613.

Cousens, B. L., R. L. Chase, and J. -G. Schilling (1984), Basalt geochemistry of the Explorer Ridge area, northeast Pacific Ocean, *Can. J. Earth Sci.*, *31*, 157–170.

Curewitz, D., and J. A. Karson (1998), Geological consequences of dike intrusion at mid-ocean ridge spreading centers, in *Faulting and Magmatism at Mid-Ocean Ridges*, edited by W. R. Buck, et al., pp. 117–136, American Geophysical Union, Washington, D.C.

Davis, E. E., and R. P. Riddihough (1982), The Winona Basin: Structure and tectonics, *Can. J. Earth Sci.*, *19*, 767–788.

Davis, E. E., R. G. Currie, B. S. Saywer, and D. M. Hussong (1984), Juan de Fuca Ridge Atlas: SEAMARC II, Acoustic Imagery, in *Energy*, *Mines and Resources Canada*, *Open File*, 84–17.

De Chabalier, J. B., and J. P. Avouac (1994), Kinematics of the Asal rift (Djibouti) determined from the deformation of Fieale volcano, *Science*, *265*(5179), 1677–1681.

Delaney, P. T., and D. D. Pollard (1982), Solidification of basaltic magma during flow in a dike, *Am. J. Sci.*, *282*, 856–885.

Deschamps, A., T. Fujiwara, M. Asada, L. Montési, and P. Gente (2005), Faulting and volcanism in the axial valley of the slow spreading center of the Mariana back-arc basin from Wadatsumi side-scan sonar images, *Geochem. Geophys. Geosyst.*, *6*, 1. doi:10.1029/2004GC000881.

Deschamps, A., M. Tivey, R. W. Embley, and W. W. Chadwick (2007), Quantitative study of the deformationnext term at Southern Explorer Ridge using high-resolution bathymetric data, *Earth Planet. Sci. Lett.*, *259*, 1–2.

Embley, R. W., et al. (2002), Rediscovery and Exploration of Magic Mountain, Explorer Ridge, NE Pacific, *Eos Trans. AGU*, *83*(47), Fall Meet. Suppl., Abstract T11C-1264.

Engels, J. L., M. H. Edwards, D. J. Fornari, M. R. Perfit, and J. R. Cann (2003), A new model for submarine volcanic collapse formation, *Geochem. Geophys. Geosyst.*, *4*(8), 1069.

Fornari, D. J., R. M. Haymon, M. R. Perfit, T. K. P. Gregg, and M. H. Edwards (1998), Geological characteristics and evolution of the axial zone on fast spreading mid-ocean ridges: Formation of an axial summit trough along the East Pacific Rise, 9°–10°N, *J. Geophys. Res.*, *103*, 9,827–9,855, http://dx.doi.org/10.1029/98JB00028.

Fox, C. G., H. Matsumoto, and T. A. Lau (2001), Monitoring Pacific Ocean seismicity from an autonomous hydrophone array, *J. Geophys. Res.*, *106*, 4183–4206.

Fundis, A. T., S. A. Soule, D. J. Fornari, and M. R. Perfit (2010), Paving the seafloor: volcanic emplacement processes during the 2005–2006 eruptions at the fast-spreading East Pacific Rise, 9°50'N, *Geochem. Geophys. Geosyst.*, *11*. doi:10.1029/2010GC003058.

Gregg, T. K. P., and J. H. Fink (1995), Quantification of submarine lava-flow morphology through analog experiments, *Geology*, *23*(1), ISSN: 0091–7613.

Gudmundsson, A. (1992), Formation and growth of normal faults at the divergent plate boundary in Iceland, *Terra Nova*, *4*, 464–471.

Head, J. W., III, L. Wilson, and D. K. Smith (1996), Mid-ocean ridge eruptive vent morphology and substructure: Evidence for dike widths, eruption rates, and evolution of eruptions and axial volcanic ridges, *J. Geophys. Res.*, *101*(B12), 28,265–28,280. doi:10.1029/96JB02275.

Jakuba, M., D. R. Yoerger, W. W Chadwick, A. M. Bradley, and R. Embley (2002), Multibeam Sonar Mapping of the Explorer Ridge with an Autonomous Underwater Vehicle, *Eos Trans. AGU*, *83*(47), Fall Meet. Suppl., Abstract T11C-1266.

Kappel, E. S., and W. B. F. Ryan (1986), Volcanic episodicity and a non-steady state rift valley along northeast Pacific spreading centers: Evidence from SeaMARC I, *J. Geophys. Res.*, *91*, 13,925–13,940.

Lister, G. S., M. A. Etheridge, and P. A. Symonds (1986), Detachment faulting and the evolution of passive continental margins, *Geology*, *14*, 246–250.

Luyendyk, B. P., and K. C. Macdonald (1977), Physiography and structure of the inner floor of the FAMOUS rift valley: observations with a deep-towed instrument package, *Geol. Soc. Am. Bull.*, *88*(4), 648–663.

Macdonald, K. C., and P. J. Fox (1988), The axial summit graben and cross-sectional shape of the East Pacific Rise as indicators of axial magma chambers and recent volcanic eruptions, *Earth Planet. Sci. Lett.*, *88*, 119–131.

Macdonald, K. C., J. -C. Sempere, and P. J. Fox (1984), East Pacific Rise from Siqueiros to Orozco fracture zones: along-strike continuity of axial neovolcanic zone and structure and evolution of overlapping spreading centers, *J. Geophys. Res.*, *89*, 6049–6069.

McConachy, T. F., and S. D. Scott (1987), Real-time mapping of hydrothermal plumes over southern Explorer Ridge, NE Pacific Ocean, *Marine Mining*, *6*, 181–204.

Michael, P. J. (1988), The concentration, behavior and storage of H2O in the suboceanic upper mantle: implications for mantle metasomatism, *Geochim. Cosmochim. Acta*, *52*, 555–566.

Michael, P. J., R. L. Chase, and J. F. Allan (1989), Petrologic and geologic variations along the Southern Explorer Ridge, Northeast Pacific Ocean, *J. Geophys. Res.*, *94*(B10), 13,895–13,918.

Michael, P. J., R. L. Chase, G. T. Shea, and T. O'Hearn (1985), Petrology and tectonics of the southern Explorer Ridge, *Geol. Soc. Am. Bull.*, *17*, 393.

Morley, C. K. (1995), Developments in the structural geology of rifts over the last decade and their impact on hydrocarbon exploration, in Hydrocarbon Habitat in Rift Basins, edited by J. J. Lambiase, *Geol. Soc. Spec. Publ.*, *80*, 65– 77.

Mutter, J. C., R. L. Larson, and N. A. S. Group (1989), Extension of the Exmouth Plateau, offshore northwestern Australia: Deep seismic reflection/refraction evidence for simple and pure shear mechanisms, *Geology*, *17*, 15–18.

Parson, L. M. *et al.* (1993), En échelon axial volcanic ridges at the Reykjanes Ridge: a life cycle of volcanism and tectonics, *Earth Planet. Sci. Lett.*, *117*, 73–87.

Patton, T. L., A. R. Moustafa, R. A. Nelson, and A. S. Abdine (1994), Tectonic evolution and structural setting of the Suez rift, in *Interior Rift Basins*, edited by S. M. Landon, AAPG Mem., 58, 9– 55.

Perfit, M. R., and W. W. Jr. Chadwick (1998), Magmatism at mid-ocean ridges: Constraints from volcanological and geochemical investigations, in *Faulting and Magmatism at Mid-Ocean Ridges*, *Geophys. Monograph 106*, edited by W. R. Buck, *et al.*, pp. 59–116, American Geophysical Union, Washington, D.C.

Pollard, D. D., P. T. Delaney, W. A. Duffield, E. T. Endo, and A. T. Okamura (1983), Surface deformation in volcanic rift zones, *Tectonophysics*, *94*, 541–584.

Richter, D. H., J. P. Eaton, K. J. Murata, W. U. Ault, and H. L. Krivoy (1970), Chronological narrative of the 1959–60 eruption of Kilauea Volcano, Hawaii: A detailed and pictorial account of an eruptive sequence consisting of a summit eruption, a flank eruption, and a summit collapse, *U.S. Geological Survey Professional Paper 537-E*, 73 p.

Riddihough, R. P. (1974), Recent movements of the Juan de Fuca plate system, *J. Geophys. Res.*, *89*, 6980–6997.

Rubin, A. (1992), Dike-Induced Faulting and Graben Subsidence in Volcanic Rift Zones, *J. Geophys. Res.*, *97*(B2), 1839–1858.

Rubin, A. M., and D. D. Pollard (1988), Dike-induced faulting in rift zones of Iceland and Afar, *Geology*, *16*, 413–417.

Sauter, D., H. Whitechurch, M. Munschy, and E. Humler (1991), Periodicity in the accretion process on the Southeast Indian Ridge at 27°40'S, *Tectonophysics*, *195*, 47–64.

Scott, S. D., R. L. Chase, M. D. Hannington, P. J. Michael, T. F. McConachy, and G. T. Shea (1990), Sulphide deposits, tectonics and petrogenesis of Southern Explorer Ridge, northeast Pacific Ocean, in *Ophiolitees and Oceanic Lithosphere*: *Proceedings of the Troodos '87 Symposium*, edited by J. Malpas, E. M. Moores, A. Panayootou, and C. Xenophontos, Geological Survey of Cyprus, Nicosia, pp. 719–733.

Smith, D. K., S. E. Humphris, M. A. Tivey, and J. R. Cann (1997), Viewing the morphology of the Mid-Atlantic Ridge from a new perspective, *EOS Trans. AGU*, *78*, 265–269.

Smith, M. C., M. R. Perfit, and I. R. Jonasson (1994), Petrology and geochemistry of basalts from the southern Juan de Fuca: controls on the spatial and temporal evolution of mid-ocean ridge basalt, *J. Geophys. Res.*, *99*, 4787–4812.

Stakes, D. S., M. R. Perfit, M. A. Tivey, D. W. Caress, T. M. Ramirez, and N. Maher (2006), The Cleft revealed: Geologic, magnetic, and morphologic evidence for construction of upper oceanic crust along the southern Juan de Fuca Ridge, *Geochem. Geophys. Geosyst.*, *7*(4), Q04003, doi:10.1029/2005GC001038.

Sturkell, E., and F. Sigmundsson (2000), Continuous deflation of the Askja caldera, Iceland, during the 1983–1998 noneruptive period, *J. Geophys. Res.*, *105*(B11). doi:10.1029/2000JB900178.

Tivey, M. A., R. Embley, W. Chadwick, A. Bradley, and D. Yoerger (2002), High-Resolution Magnetic Field Mapping Over Explorer Ridge - NOAA Ocean Exploration Program, *EOS Trans. AGU* (Fall Meeting), *83*(47), T11C-1267.

Tucholke, B. E., and J. Lin (1994), A geological model for the structure of ridge segments in slow spreading ocean crust, *J. Geophys. Res.*, *99*(B6), 11937–11958. doi:10.1029/94JB00338.

Tunnicliffe, V., M. Botros, M. E. Deburgh, A. Dinet, H. P. Johnson, S. K. Juniper, and R. E. McDuff (1986), Hydrothermal vents of the Explorer Region, Northeast Pacific, *Deep Sea Res.*, *33*, 401–412.

Wernicke, B. (1985), Uniform-sense normal simple shear of the continental lithosphere, *Can. J. Earth Sci.*, *22*, 108–125.

Wernicke, B., and B. C. Burchfiel (1982), Modes of extensional tectonics, *J. Struct. Geol.*, *4*, 105–115.

White, S. M., K. C. Macdonald, and R. M. Haymon (2000), Basaltic lava domes, lava lakes, and volcanic segmentationon the southern East Pacific Rise, *J. Geophys. Res.*, *105*(B10), 23519–23536.

Wilcock, W. S. D., and J. R. Delaney (1996), The size of mid-ocean ridge sulfide deposits: Evidence for heat extraction from magma chambers or cracking fronts, *Earth Planet. Sci. Lett.*, *145*, 49–64, doi:10.1016/S0012-821X(96)00195-1.

Yoerger, D. R., A. Bradley, M. -H. Cormier, W. B. F. Ryan, and B. Walden (1999), High resolution mapping of a fast spreading mid ocean ridge with the Autonomous Benthic Explorer, *Proceedings of the 11th International Symposium on Unmanned Untethered Submersible Technology*, Durham, NH, 14 pp.

Yoerger, D. R., A. Bradley, B. Walden, H. Singh, and R. Bachmayer (1997), Surveying a subsea lava flow using the Autonomous Benthic Explorer (ABE), *J. Japan Soc. Marine Surveys Technol.*, *9*(1), 43–60.